Bioconjugate Chemistry

Article

pubs.acs.org/bc

Effect of Attachment Site on Stability of Cleavable Antibody Drug Conjugates

Magdalena Dorywalska,[†] Pavel Strop,*[,†] Jody A. Melton-Witt,[†] Adela Hasa-Moreno,[†] Santiago E. Farias,[†] Meritxell Galindo Casas,[†] Kathy Delaria,[†] Victor Lui,[†] Kris Poulsen,[†] Carole Loo,[†] Stellanie Krimm,[†] Gary Bolton,[†] Ludivine Moine,[‡] Russell Dushin,[‡] Thomas-Toan Tran,[†] Shu-Hui Liu,[†] Mathias Rickert,[†] Davide Foletti,[†] David L. Shelton,[†] Jaume Pons,[†] and Arvind Rajpal[†]

[†]Rinat Laboratories, Pfizer Inc., 230 East Grand Avenue, South San Francisco, California 94080, United States

[‡]Worldwide Medicinal Chemistry, Pfizer Inc., 445 Eastern Point Road, Groton, Connecticut 06340, United States

Supporting Information

ABSTRACT: The systemic stability of the antibody−drug linker is crucial for delivery of an intact antibody−drug conjugate (ADC) to target-expressing tumors. Linkers stable in circulation but readily processed in the target cell are necessary for both safety and potency of the delivered conjugate. Here, we report a range of stabilities for an auristatin-based payload site-specifically attached through a cleavable valine-citrulline-*p*-aminobenzylcarbamate (VC-PABC) linker across various sites on an antibody. We demonstrate that the conjugation site plays an important role in determining VC-PABC linker stability in mouse plasma, and that the stability of the linker positively correlates with ADC cytotoxic potency both in vitro and in vivo. Furthermore, we show that the VC-PABC cleavage in mouse plasma is not mediated by Cathepsin B, the protease thought to be primarily responsible for linker processing in the lysosomal degradation pathway. Although the VC-PABC cleavage is not detected in primate plasma in vitro, linker stabilization in the mouse is an essential prerequisite for designing successful efficacy and safety studies in rodents during preclinical stages of ADC programs. The divergence of linker metabolism in mouse plasma and its intracellular cleavage offers an opportunity for linker optimization in the circulation without compromising its efficient payload release in the target cell.

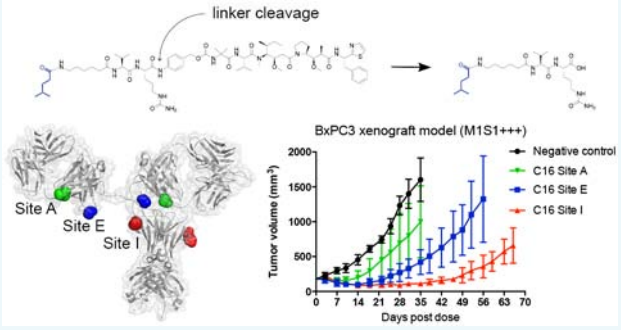

INTRODUCTION

Antibody−drug conjugates offer the advantage of delivering cytotoxic agents directly to the target-expressing cells, thus potentially improving the therapeutic efficacy and minimizing harmful side effects as compared to conventional chemotherapy.[1−3] Loss of toxin from the conjugate while in circulation can result in off-target toxicity from the released payload, and generation of an unconjugated antibody that can compete for target binding with the intact ADC, leading to loss of efficacy. Therefore, it is highly desirable that cytotoxic agents remain stably attached until the conjugate reaches the tumor, where the toxic payload may then be efficiently released into the tumor cell only after internalization.[4,5]

Previously, we described an efficient site-specific conjugation method using microbial transglutaminase to attach a wide range of cleavable and noncleavable payloads to various sites in an antibody to generate homogeneous conjugates with unique properties.[6−8] In this approach, a glutamine-containing tag (LLQG) was engineered into selected positions in an antibody sequence, and microbial transglutaminase was used to catalyze transamidation reaction between the glutamine γ-carboxamide group and a primary amine of the payload of choice, creating a covalent isopeptide bond. The selected sites were shown to be transferrable among several different antibodies. We further showed that the glutamine tag engineered into the antibody sequence, as well as the transglutaminase-catalyzed isopeptide linkage between the engineered antibody and the payload, remain intact upon exposure to rodent serum in vitro and upon administration in vivo. We did, however, detect plasma cleavage of the VC-PABC linker resulting in a loss of the payload moiety.[7] Here, we investigate the stability of a cleavable linker-payload conjugated at a wide range of positions, its dependence on the site of conjugation, and the correlation of stability with efficacy in vitro and in vivo. While the site of attachment has previously been shown to modulate stability of maleimide-based conjugates, the effect was due to chemical decoupling of the maleimide linkage[9] rather than the enzymatic processing of the VC-PABC linker during circulation. We further examine the cleavage of the VC-PABC linker resulting in the loss of an auristatin-based payload from a mechanistic perspective to gain insight into the plasma enzyme(s) responsible for this process.

Received: December 5, 2014
Revised: January 27, 2015
Published: February 2, 2015

DOI: 10.1021/bc5005747
Bioconjugate Chem. 2015, 26, 650−659

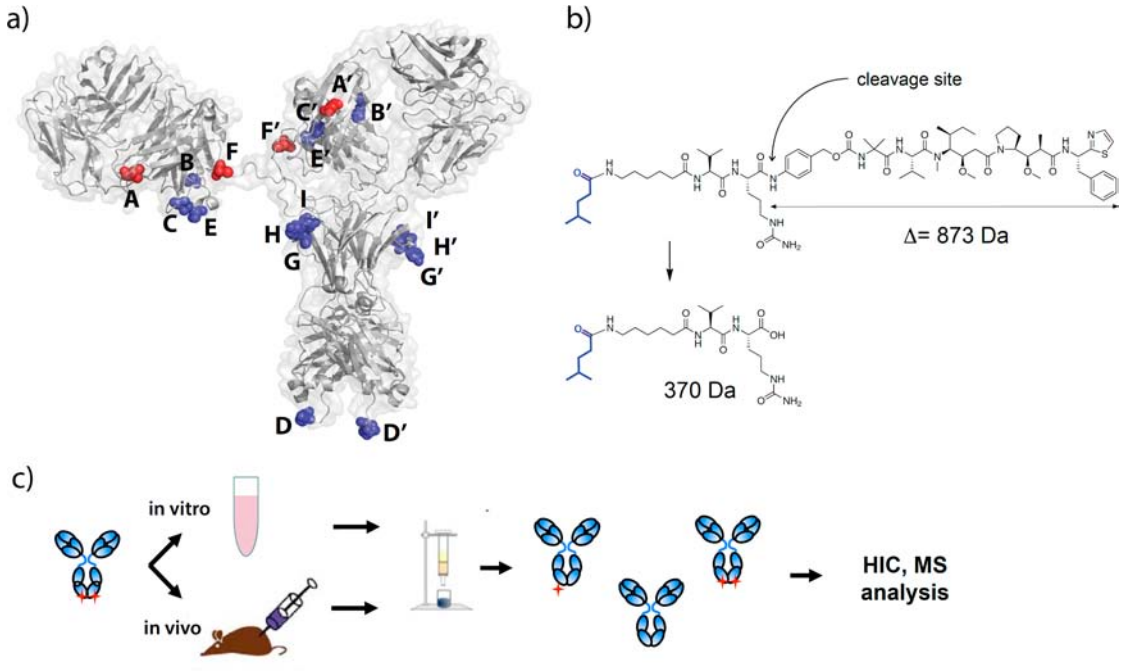

Figure 1. Stability studies of site-specific cleavable ADCs. (a) Positions of conjugation sites on an antibody. (b) Structure of the cleavable C6-VC-PABC-Aur0101 payload conjugated to the glutamine tag on the antibody, and its cleavage product. The glutamine residue is shown in blue. (c) Experimental setup for in vitro and in vivo ADC stability assays.

RESULTS

Stability and Cytotoxic Potency of Cleavable Conjugates in Vitro. Earlier studies of transglutaminase-based conjugates revealed the significant role played by the conjugation site in determining the stability and pharmacokinetic properties of ADCs.[7] To further evaluate linker-payload stability across a number of conjugation sites (Figure 1a), we generated a series of site-specific conjugates using an auristatin-based cleavable linker-payload, Aminocaproyl-VC-PABC-Aur0101 (C6-VC-PABC-Aur0101, Scheme 1)[10] conjugated to a glutamine residue (Figure 1b) that had been engineered into anti-M1S1 antibody C16 using site directed mutagenesis at selected positions (Figure 1a, Table 1). The conjugates were incubated in the blood plasma of several species, followed by purification and analysis of their drug loading using hydrophobic interaction chromatography (HIC) and mass spectrometry (Figure 1c). While the isopeptide linkage resulting from transglutaminase conjugation was intact across all sites and all species, in mouse plasma we observed cleavage of the VC-PABC linker resulting in the loss of the hydrophobic PABC-Aur0101 moiety (Figure 1b), and a shift toward lower retention time on HIC (Supporting Information Figure 1). Mass spectrometric analysis following incubation in mouse plasma reveals a corresponding 873 Da mass loss from the ADC (Figure 1b, Figure 2a,b, Supporting Information Figure 2). This cleavage appears to be at the same Cit-PABC amide bond as occurs through normal processing in lysosomal compartments that leads to payload release in target cells.[11−13] The VC-PABC linker is cleaved in this way to a varying extent at different sites on either heavy and/or light chains of the antibody when incubated in mouse plasma from either Balb/c or SCID strains, but appears to be more stable in rat, cynomolgus monkey, and human plasma (Table 1). The wide range of mouse plasma stabilities across conjugation sites suggests varied degrees of protection of the linker from proteolytic cleavage through steric hindrance by adjacent antibody domains.

Linker stability is a key determinant of ADC potency which relies on the efficient linker processing and payload release inside target cells and, at the same time, the exquisite systemic stability prior to internalization. To examine how the differential C6-VC-PABC-Aur0101 linker stability across conjugation sites correlates with the cytotoxic activity of the ADCs, we performed in vitro cytotoxicity assays using C16 conjugates before and after incubation in mouse plasma. All of the untreated C6-VC-PABC-Aur0101 conjugates showed comparable and target specific potency against the BxPC3 cell line (M1S1+++) demonstrating an efficient mechanism of intracellular payload release at all conjugation sites (Figure 3a−c, Supporting Information Figure 3a,c and Table 1). Lack of efficacy from a nonbinding, negative control conjugate NCC Site F-C6-VC-PABC-Aur0101 verified that target recognition and conjugate internalization are required for specific cell killing (Supporting Information Figure 3b). Target specificity was also demonstrated using the SW620 cell line that does not express M1S1 (Supporting Information Figure 3c). In contrast to untreated conjugates which show similar anti-BxPC3 IC_{50} values (0.6−1.2 nM), ADCs purified after a 4.5 day incubation in mouse plasma showed varying degrees of potency decrease that correlated with their VC-PABC linker instability, with the most stable Site I-C6-VC-PABC-Aur0101 conjugate showing no change in the IC_{50} value after plasma exposure (IC_{50} before and after exposure of 1.0 and 0.9 nM, respectively), and the least stable Site A-C6-VC-PABC-Aur0101 conjugate showing significantly reduced cytotoxicity (IC_{50} changed from 1.2 nM for untreated conjugate to ≥266 nM after treatment) (Figure 3a−c, Supporting Information Figure 3a and Table 1). Establishing an exact quantitative dependence between ADC potency and linker stability is not possible due to the presence of other factors that affect ADC activity (such as internalization rates, possible differential intracellular processing by lysosomal proteases), all of which are functions of time. Nevertheless, the qualitative correlation between stability and potency can be seen

DOI: 10.1021/bc5005747
Bioconjugate Chem. 2015, 26, 650−659

Table 1. Stability of the Cleavable C6-VC-PABC-Aur0101 Conjugate Series under Various Conditions[a]

site	position	payload	mouse plasma stability (%)	rat plasma stability (%)	cyno plasma stability (%)	human plasma stability (%)	mouse in vivo stability (%)
A	LC 200−202	C6-VC-PABC-Aur0101	5	94	99	99	0
B	HC 160	C6-VC-PABC-Aur0101	12	99	100	100	-
C	HC 135	C6-VC-PABC-Aur0101	22	97	98	96	-
D	HC C-terminus	C6-VC-PABC-Aur0101	34	97	99	100	-
E	HC 190−192	C6-VC-PABC-Aur0101	42	97	97	100	0
F	LC C-terminus	C6-VC-PABC-Aur0101	86	99	100	98	-
G	N297A	C6-VC-PABC-Aur0101	88	100	99	100	-
H	N297Q	C6-VC-PABC-Aur0101	100	100	100	100	-
I	HC 294−297	C6-VC-PABC-Aur0101	100	100	100	100	57

[a]Stability values are calculated as the ratio of drug loading after treatment and before treatment, and expressed as a percentage. Calculations are based on DAR values obtained from HIC analysis for most conjugates, except for Site G, H, and I conjugates for which DAR values are determined by mass spec analysis. Both methods give consistent DAR values; however, HIC chromatograms of Site G, H, and I conjugates show insufficient shift between DAR 0, 1, and 2 peaks for accurate integration.

Scheme 1. [a]

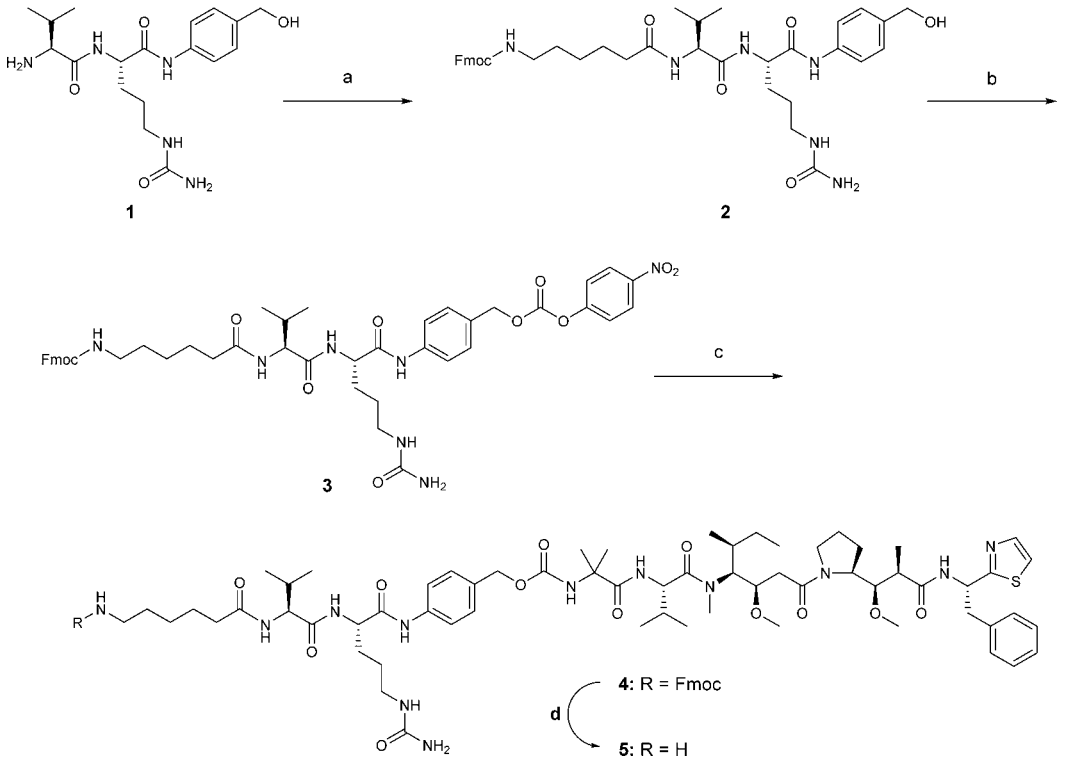

[a]Reagents and conditions: (a) Fmoc-aminohexanoic acid, HATU, *i*-Pr_2NEt, DMF; (b) (*p*-NO_2-Ph)$_2$CO, *i*-Pr_2NEt, DMF; (c) Aur-0101, HOAT, 2,6-lutidine, DMF; (d) piperidine.

when stability is plotted against in vitro cytotoxicity data (Supporting Information Figure 4).

In Vivo Efficacy and Its Relation to Stability of Cleavable ADCs. To evaluate whether the in vitro VC-PABC linker stability differences observed in the mouse plasma translate into differences in antitumor efficacy, we selected three C16 conjugates for comparative in vivo efficacy study: the unstable Site A-C6-VC-PABC-Aur0101, the intermediate stability Site E-C6-VC-PABC-Aur0101, and the stable Site I-C6-VC-PABC-Aur0101. A single intravenous dose of the three conjugates given to mice implanted with BxPC3 cells resulted in varying degrees of tumor growth inhibition or tumor regression that correlated with the VC-PABC linker stability observed in vitro (Figure 3d). The NCC Site F-C6-VC-PABC-Aur0101 conjugate was used as a negative control to monitor tumor response to nontargeting conjugate present in the circulation (Figure 3d). A pharmacokinetic study in non-tumor-bearing mice verified that the observed efficacy differences among the conjugates were not a result of different whole antibody exposure as demonstrated using total antibody ELISA (Figure 3e). Instead, the efficacy differences can be attributed to differential amount of drug loss resulting in different ADC exposure (Figure 3e). These data suggest that a kinetic competition between the rate of VC-PABC cleavage in the plasma and the rate of cell killing by the ADC, even in the early days post dosing, will have a significant effect on the antitumor outcome of the treatment.

The varying extent of PABC-Aur0101 payload loss in vivo was confirmed by isolating the three conjugates from non-tumor-bearing

DOI: 10.1021/bc5005747
Bioconjugate Chem. 2015, 26, 650−659

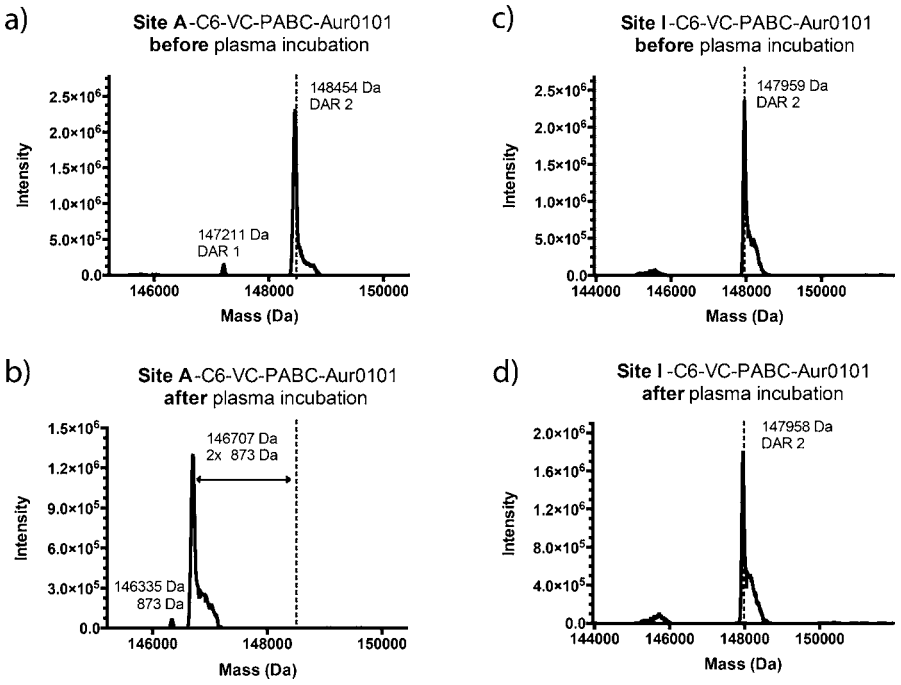

Figure 2. Mass spectrometric analysis of cleavable conjugates before (a and c) and after (b and d) incubation in mouse plasma. The figure labels represent experimentally observed masses. (a) Intact mass deconvolution of C16 Site A-C6-VC-PABC-Aur0101 conjugate before plasma incubation. The mass difference between the peak representing drug to antibody ratio of 1 (DAR 1) and DAR 2 is approximately 1243 Da which corresponds to the mass of the cytotoxic drug plus the linker (less ammonia). (b) Intact mass analysis of C16 Site A-C6-VC-PABC-Aur0101 conjugate after plasma exposure. Cleavage by a plasma protease results in a loss of 873 Da from each conjugated payload, shifting the DAR 2 peak by 2 × 873 Da, and the DAR 1 peak by 1 × 873 Da. (c) Intact mass deconvolution of C16 Site I-C6-VC-PABC-Aur0101 conjugate before plasma incubation. The observed DAR 2 peak represents the mass of the antibody conjugated to two linker-payload molecules. (d) Intact mass analysis of C16 Site I-C6-VC-PABC-Aur0101 conjugate after mouse plasma treatment. No mass difference is observed for this conjugate, indicating a high degree of stability in mouse plasma.

mice at 4.5 days after a 3 mg/kg dose, and evaluating their drug loading using HIC and mass spectrometry (Table 1). We note that in mice the VC-PABC linker appears to be cleaved more efficiently in vivo relative to the in vitro assay. This could be a result of a continuous source of putative enzyme(s) in vivo, or alternatively due to a contribution from intracellular cleavage and release of the unconjugated antibody through endocytic recycling. Target-mediated recycling is unlikely in this case, since the C16 antibody does not recognize the mouse M1S1 protein in non-tumor-bearing mice. While we detect only low levels of VC degradation in rat plasma, and practically none in monkey or human plasma in vitro assays (Table 1), the loss of payload due to VC-PABC cleavage from a related C16 Site D-C6-VC-PABC-MMAD conjugate was observed in pharmacokinetic studies in both rat and cynomolgus monkey (Supporting Information Figure 5).

Mechanistic Comparison of VC-PABC Cleavage in Mouse Plasma to Cathepsin B Activity. To determine whether an enzymatic mechanism is responsible for the hydrolysis of the VC-PABC linker in the mouse plasma, we conducted thermal inactivation, protease inhibitor, and pH dependence studies. Preincubation of mouse plasma at 65 °C for 1 h completely abolished its VC-PABC cleavage activity (data not shown), suggesting that the VC metabolism in plasma is a result of a thermo-labile enzymatic process. Next, we investigated whether the cleavage of the VC-PABC linker in the plasma occurs through the activity of Cathepsin B, one of the key endosomal/lysosomal cysteine proteases believed to be responsible for intracellular VC-PABC cleavage and toxin release.[11,14,15] While Cathepsin B is not thought to be prevalent in the plasma of healthy individuals, increased extracellular levels of the enzyme and other cysteine cathepsins have been described in various pathological states such as neurodegenerative disease, arthritis, and tumorigenic and metastatic pathways.[16−22]

All of the described cleavable C6-VC-PABC-Aur0101 C16 conjugates displayed comparable in vitro efficacy profiles against target positive BxPC3 cells (Figure 3a−c, Supporting Information Figure 3a and Table 1), suggesting comparable intracellular processing and payload release for each of the examined sites on the time scale of the cytotoxicity assay (4 days). However, the cleavage of the VC-PABC linker in mouse plasma was distinctly dependent on the conjugation site (Table 1). Therefore, we selected the least stable C16 conjugate, Site A-C6-VC-PABC-Aur0101, as a substrate for enzymatic characterization assays. In a series of comparative assays, the substrate was incubated under the conditions described in the presence of purified Cathepsin B or plasma from mouse or human, followed by HIC analysis to assess the extent of VC-PABC linker cleavage and payload loss. The Site A-C6-VC-PABC-Aur0101 substrate underwent a complete cleavage in the presence of mouse or human Cathepsin B over a 20 h incubation at either pH 5.2 or 6.0; however, both enzymes showed negligible activity at pH 7.4 or higher (Table 2). This observation is consistent with the expectation that endosomal/lysosomal proteases, including Cathepsin B, have a pH optimum in the acidic range.[23] In contrast, incubation of the substrate in the mouse plasma at 37 °C for 20 h resulted in an efficient VC-PABC cleavage over a wide range of pH from 5.2 to 8.5 (Table 2). We did not detect any proteolytic activity upon incubation of the VC-PABC substrate in human plasma in vitro, suggesting that either human plasma does not contain the responsible hydrolase(s) or the human enzyme is inactive or inhibited under conditions used in the in vitro assay.

DOI: 10.1021/bc5005747
Bioconjugate Chem. 2015, 26, 650−659

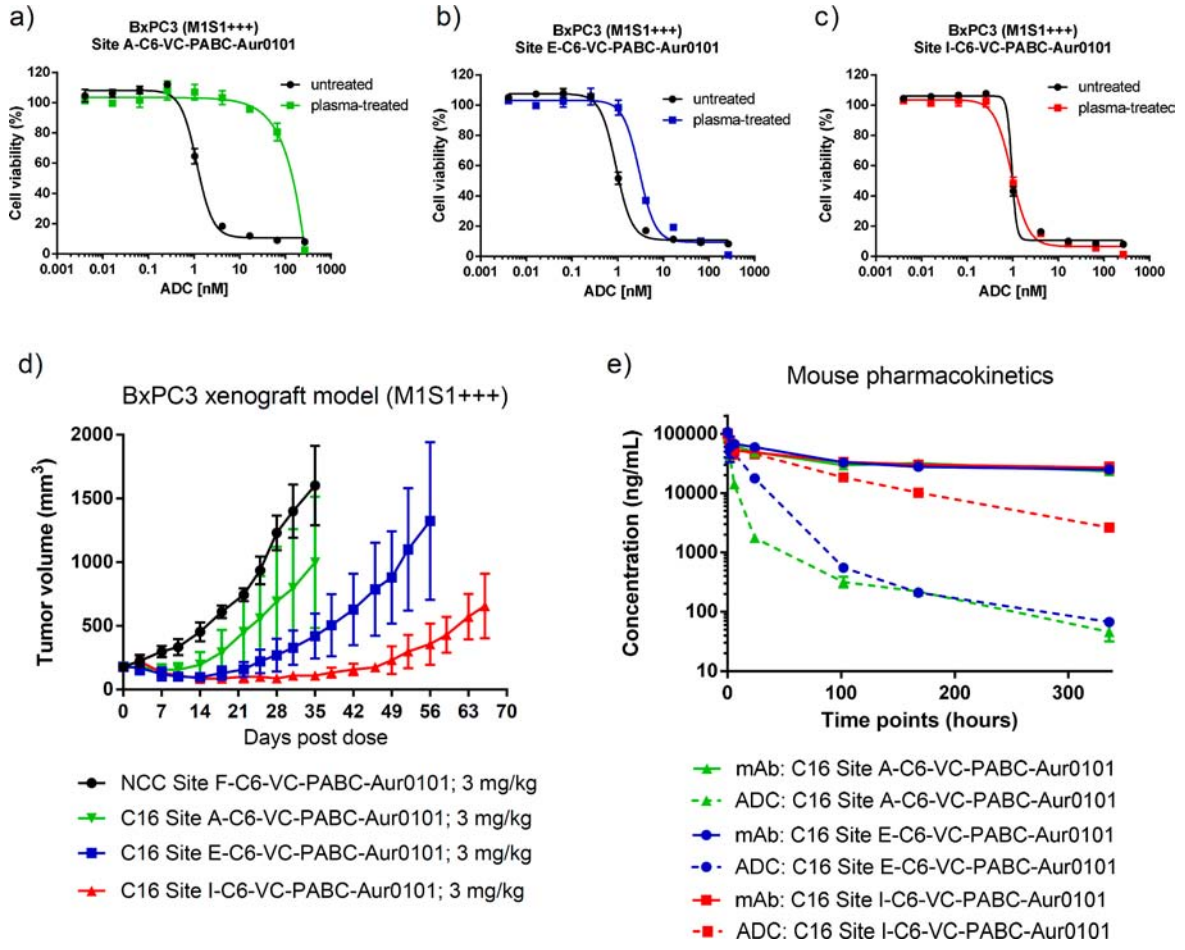

Figure 3. Comparative efficacy studies of cleavable ADCs. Comparison of in vitro cytotoxic activities of untreated and plasma-treated anti-M1S1 cleavable conjugates against BxPC3 cells (M1S1+++). (a) Plasma-sensitive C16 Site A-C6-VC-PABC-Aur0101 conjugate. (b) C16 Site E-C6-VC-PABC-Aur0101 conjugate with intermediate plasma stability. (c) Stable conjugate C16 Site I-C6-VC-PABC-Aur0101. (d) In vivo comparison of the three conjugates in the BxPC3 xenograft model, along with a negative control conjugate NCC Site F-C6-VC-PABC-Aur0101. All compounds were dosed at 3 mg/kg. (e) Mouse pharmacokinetic profiles of the three conjugates. Solid lines represent total antibody ELISA, while dashed lines show antidrug ELISA. All compounds were given as single dose at 3 mg/kg.

Table 2. Testing pH Dependence and Protease Inhibitor Sensitivity of the A-C6-VC-PABC-Aur0101 Linker Cleavage by Mouse and Human Cathepsin B in Comparison with Mouse and Human Plasma[a]

pH	inhibitor	mouse cathepsin B stability (%)	human cathepsin B stability (%)	mouse plasma stability (%)	human plasma stability (%)
5.2	-	0	0	47	100
6.0	-	0	0	45	100
7.4	-	95	94	47	100
8.5	-	100	100	42	100
6.0	E64, 10 μM	99	100	44	-
6.0	Leupeptin, 10 μM	90	76	44	-
6.0	Pefabloc, 1 mM	0	0	100	-

[a]The A-C6-VC-PABC-Aur0101 cleavage activity is expressed in terms of ADC stability values which are given as percentage. The incubation time was decreased to 20 h to capture any differences between Cathepsin B and plasma cleavage under various conditions.

To further investigate whether the cleavage of the VC-PABC linker in mouse plasma occurs through a Cathepsin B-independent mechanism, we employed a series of protease inhibition assays. The purified mouse and human Cathepsin B showed a reduced VC-PABC cleavage when incubated at pH 6.0 in the presence of protease inhibitor E64 (known to inhibit primarily cysteine proteases including Cathepsin B[14,24]) and Leupeptin (an inhibitor of cysteine and serine proteases[24]) (Table 2). In contrast, the addition of either E64 or Leupeptin to the substrate in mouse plasma had no effect on the extent of VC-PABC cleavage at either pH 6.0 or 7.4 (Tables 2 and 3). This observation further suggests that the enzymatic cleavage taking place in the mouse plasma is not mediated by Cathepsin B or a closely related cysteine protease. In further tests, the addition of Pefabloc, mainly a serine protease inhibitor,[24] had no effect on the VC-PABC cleavage by either mouse or human Cathepsin B at pH 6.0 (Table 2), but resulted in a significant inhibition of the cleavage in mouse plasma at both pH 6.0 and 7.4 (Table 2 and 3).

Among other serine protease inhibitors tested (Leupeptin, Antipain, Chymostatin, Aprotinin, Benzamidine, and 3,4-Dichloroisocoumarin[24,25]), only 3,4-Dichloroisocoumarin had a partial inhibitory effect on the VC-PABC cleavage in mouse plasma (Table 3). Inhibitors against cysteine-based hydrolases (E64, Leupeptin, Antipain, Chymostatin, and *N*-ethylmaleimide[24,25]) had no effect on the VC-PABC plasma cleavage, with the exception of partial inhibition by *N*-ethylmaleimide (Table 3). While a cysteine-based mechanism cannot be completely ruled out, it is possible that the partial sensitivity of the plasma enzyme to *N*-ethylmaleimide

DOI: 10.1021/bc5005747
Bioconjugate Chem. 2015, 26, 650−659

Table 3. Protease Inhibition Studies of the C6-VC-PABC-Aur0101 Cleavage in Mouse Plasma[a]

inhibitor	inhibitor specificity	C6-VC-PABC-Aur0101 stability in mouse plasma (%)
-	-	3
E64, 30 μM	Cys proteases and trypsin	3
Leupeptin, 100 μM	Cys & Ser proteases	4
Antipain, 100 μM	Cys & Ser proteases	4
Chymostatin, 100 μM	Cys & Ser proteases	6
N-Ethylmaleimide, 1 mM	Cys proteases	17
Aprotinin, 5 μM	Ser proteases	3
Pefabloc, 1 mM	Ser proteases	96
Benzamidine, 4 mM	Ser proteases	6
3,4-Dichloroisocoumarin, 1 mM	Ser proteases	28
Pepstatin A, 1 μM	Asp proteases	4
Bestatin, 135 μM	Metalloproteases	3
EDTA, 5 mM	Metalloproteases	5
Carboxypeptidase inhibitor, 10 μM	Carboxypeptidase A & B	4
α2-macroglobulin, 0.3 μM	Broad spectrum inhibitor	5

[a]The A-C6-VC-PABC-Aur0101 cleavage activity is expressed in terms of ADC stability values which are shown as percentage. All assays were carried out at pH 7.4.

might be due to reactivity with a cysteine, histidine, or the α-amino group of *N*-terminal residue.[26] Inhibitors of aspartate proteases (Pepstatin[24]), metalloproteases (Bestatin, EDTA[24]), and carboxypeptidases (carboxypeptidase inhibitor[25]), as well as the broad-spectrum inhibitor α2-macroglobulin[25] had no effect on the VC-PABC cleavage in mouse plasma (Table 3). These data suggest that the VC-PABC linker degradation in mouse plasma is most likely mediated by a serine hydrolase.

Interestingly, proteolysis of the Site A-C6-VC-PABC-Aur0101 conjugate by either mouse or human Cathepsin B is completely blocked upon the addition of plasma even when adjusted to pH 6.0 (Supporting Information Table 2). The loss of Cathepsin B activity in the presence of plasma could result from its inhibition or degradation by plasma components,[27] preference of Cathepsin B for other substrates that may be available in plasma, or its insufficient affinity toward the Site A-C6-VC-PABC-Aur0101 conjugate in the rich plasma environment. This observation further demonstrates that an enzyme other than Cathepsin B is likely responsible for VC-PABC cleavage in the plasma.

Taken together, our results suggest that the cleavage of the VC-PABC linker likely occurs by two independent enzymatic processes with unique characteristics: proteolysis by the lysosomal proteases such as Cathepsin B, most efficient under acidic conditions and effectively blocked by cysteine protease inhibitors, and in mouse plasma by a novel enzymatic activity attributed to an unidentified extracellular hydrolase. The plasma hydrolase activity shows less dependence on pH, and is sensitive to serine hydrolase inhibitors Pefabloc and 3,4-Dichloroisocoumarin. The existence of a distinct enzymatic process responsible for the VC-PABC linker instability in the plasma opens up the possibility to remedy this liability without affecting the desired ADC processing and payload release in the endosomal/lysosomal compartment of the target cell.

DISCUSSION AND CONCLUSIONS

The rapidly expanding field of antibody−drug conjugates for cancer therapy has relied on the properties of linkage chemistries which ideally would offer both a stable toxin attachment to the antibody while in the systemic circulation and an efficient release by intracellular proteases. Cleavable linker technologies designed to undergo drug release in response to pH or reducing environment show relatively poor in vivo stability compared to peptide-based linkers.[5,28,29] While the widely popular valine-citrulline based linkers have been thought to be stable in the plasma environment, payload loss has been reported to occur through the decoupling of thiosuccinimide linkages from conjugates generated through cysteine−maleimide methods.[9,30] The maleimide linkage stability was reported to be dependent on solvent accessibility and local environment, and has been demonstrated to be enhanced by forced or spontaneous maleimide ring opening.[9,31,32]

Alternative conjugation method utilizing microbial transglutaminase produces a site-specific and stable amide linkage between a primary amine of the linker-payload and a glutamine side chain on the antibody. The linkage remains intact upon prolonged exposure to plasma environment (both in vitro and in vivo) and allowed us to examine the stability of the remainder of the linker-payload. We report a wide range of plasma stabilities of ADCs bearing cleavable linker-payloads, with stability varying across specific locations throughout the antibody.

Our data suggest that the C6-VC-PABC-Aur0101 cleavage occurs most readily in mouse plasma, and is mediated by an alternative enzymatic entity than the endosomal/lysosomal protease Cathepsin B with altered pH preference and different protease inhibitor sensitivity. In the rat, the VC-PABC cleavage is more efficient in the circulation in vivo than in the plasma assays in vitro. In our experiments, we did not detect any VC-PABC proteolytic activity on the tested conjugates in human or cynomolgus monkey plasma in vitro; however, we observed some level of drug loss from a related C6-VC-PABC-MMAD conjugate in the monkey in vivo samples. While the problem of premature VC-PABC degradation in the circulation appears more severe in rodents than in primates so far, the time dependent toxin loss in the rodent plasma confounds understanding of relative efficacy and safety across various species. Clarifying these differences and controlling the cleavage mechanism to optimize ADC stability in the mouse and rat is essential since preclinical efficacy and safety studies typically utilize rodent species.

Our results demonstrate that site selection is an important step in the design of systemically stable cleavable auristatin-based conjugates, offering the means to overcome inherent linker instability. The VC-PABC linker proteolysis in the mouse plasma shows a strong dependence on the site of conjugation, implicating either local environment or steric hindrance by proximal antibody domains may play a role in protecting the VC-PABC linker from proteolytic cleavage. The site of attachment can have a dramatic impact on the conjugate stability both in vitro and in vivo, and consequently on conjugate potency. These observations are in line with previous studies describing the effect of conjugation site on ADC properties, including linker stability and drug exposure,[7,9] and further highlight the advantage of site-specific conjugation methods that permit generation of a homogeneous population of ADCs with the desired properties. We were able to identify positions on the antibody that are protective of the labile VC-PABC-containing linker, and narrowed down the potential hydrolases that are likely responsible for the cleavage in circulation. We expect that the VC-PABC degradation in the plasma is not unique to the transglutaminase-based cleavable conjugates, and that the cleavage will be observed at susceptible positions when other stable conjugation chemistries are utilized.[33] Future studies will focus on identification of the

DOI: 10.1021/bc5005747
Bioconjugate Chem. 2015, 26, 650−659

plasma hydrolase and deciphering how cleavable VC-PABC linkers can be further stabilized in circulation without compromising their intracellular processing and cytotoxic activity.

MATERIALS AND METHODS

Protein Purification. A glutamine tag was introduced at selected positions of anti-M1S1 C16 antibody through residue insertion or substitution using site directed mutagenesis as previously described.[7] The sites are as follows: Site A, light chain residues 200−202 replaced by LLQG tag; Site B, insertion of LLQG tag at position 160 in the heavy chain; Site C, insertion of LLQG tag at position 135 in the heavy chain; Site D, replacement of residue 447 with LLQGA tag in the heavy chain; Site E, heavy chain residues 190−192 replaced by LLQG tag; Site F, insertion of GGLLQGPP tag after residue 214 in the light chain; Site G, N297A deglycosylation mutant (conjugation happens at native Q295 on the heavy chain); Site H, N297Q mutant (conjugation happens on Q295 and Q297 on the heavy chain[34]); Site I, heavy chain residues 294−297 replaced with LLQG tag. Anti-M1S1 constructs were cloned into in-house expression plasmids and transiently expressed in HEK293 cells. Conditioned media was applied to Protein A MabSelect SuRe columns (GE Healthcare, Inc.) and washed with 140 mM NaCl, 2.7 mM KCl, and 10 mM PO_4^{-3} (1× PBS) until baseline was reached. Protein was eluted with 100 mM sodium citrate buffer, pH 3.5, and immediately neutralized with 800 mM sodium phosphate buffer, pH 7.4. Eluted protein was dialyzed into 1× PBS and stored at 4 °C.

CONJUGATION

For the conjugation of anti-M1S1 C16 constructs to C6-VC-PABC-Aur0101, the antibody concentration was adjusted to 5 mg/mL in buffer containing 25 mM Tris-HCl, pH 8.0, 150 mM sodium chloride. Payload was added in a 10- to 25-fold molar excess over antibody, and the enzymatic reaction was initiated by addition of 2% (w/v) bacterial transglutaminase (Ajinomoto Activa TI, Japan). Following incubation with shaking at 37 °C for 16−24 h, conjugates were purified using MabSelect SuRe (GE Healthcare, Inc.) following standard procedures. Alternatively, conjugates were purified using preparative Butyl Sepharose High Performance (Butyl HP, GE Healthcare Biosciences) by adjusting the reaction mixture to obtain a buffer composition of 0.75 M ammonium sulfate, 25 mM potassium phosphate, pH 7 (Buffer A). The material was applied to a Butyl HP column, washed with 5 column volumes of Buffer A, and eluted with a linear gradient into 25 mM potassium phosphate, pH 7. Fractions containing the ADC were pooled, dialyzed against PBS, concentrated using a 10 kDa Amicon Ultra centrifugal filter unit (Millipore Corporation), and sterile filtered through a 0.2 μm filter.

Hydrophobic Interaction Chromatography Analysis. Drug−antibody ratios (DAR) for purified conjugates and their metabolic products were evaluated using a TSK-GEL Butyl-NPR column (4.6 mm × 3.5 cm) (Tosoh Bioscience) on an Agilent HP 1100 HPLC (Agilent). The HIC method utilized a mobile phase of 1.5 M ammonium sulfate, 50 mM potassium phosphate, pH 7 for Buffer A, and 50 mM potassium phosphate, pH 7 with 20% isopropanol for Buffer B. Using a flow rate of 0.8 mL/min, ADC in 0.75 M ammonium sulfate was loaded onto the column, and eluted with a gradient consisting of a 2.5 min hold at 0% Buffer B, followed by a 35 min linear gradient into 100% Buffer B.

LC/MS Intact Mass Analysis. Prior to LC/MS analysis, conjugates and metabolites were deglycosylated with PNGase F (NEB, cat#P0704L) under nondenaturing conditions at 37 °C overnight. ADCs (500 ng) were loaded into a reverse phase column packed with a polymeric material (Michrom-Bruker, cat# CM8/00920/00). LC/MS analysis was performed using Agilent 1100 series HPLC system, comprising binary HPLC pump, degasser, thermostated auto sampler, column heater, and diode-array detector (DAD), coupled to an Orbitrap Velos Pro (Thermo Scientific) mass spectrometer with electrospray ion source. The mobile phases were composed of solvent A (water, 0.1% formic acid) and solvent B (acetonitrile, 0.1% formic acid). The HPLC was carried out using an increasing gradient of solvent B over a 30 min run, consisting of isocratic flow of 3% solvent B for 10 min, followed by a gradient up to 97% solvent B over 1 min, held at 97% solvent B for 2 min, and followed finally with an equilibration step at 3% solvent B for 17 min. The charge state envelopes corresponding to the ADCs were deconvoluted using ProMass software (Thermo Fisher Scientific) to determine the masses.

LC/MS/MS Analysis of ADC Tryptic Digestions. ADCs (100 μg) were solubilized in 0.2% RapiGest (Waters Corp, 186001861) in 20 mM ammonium bicarbonate. The samples were then incubated at 80 °C for 15 min. Dithiothreitol (DTT, 20 mM final concentration) was added and the samples were incubated at 60 °C for 30 min to reduce disulfide bonds. After the samples were cooled to room temperature, iodoacetamide (IAA, 15 mM final concentration) was added, and samples were incubated at room temperature for 30 min in the dark to alkylate reduced cysteines. Modified trypsin (Promega, cat#V5111) was added (1:100 enzyme/substrate) and the samples were incubated at 37 °C overnight. To hydrolyze the RapiGest prior to mass spectrometry analysis, TFA was added to a final concentration of 60 mM, and the solution was incubated at 37 °C for 45 min, and then centrifuged at 20 800 *g* at 4 °C for 30 min. Samples (2.5 μg of digested protein) were loaded into an Agilent Poroshell 120 C18 column (2.1 × 100 mm, 2.7 μm), and eluted at 45 °C with a flow rate of 0.3 mL/min. LC/MS/MS analysis was performed using Agilent 1100 series HPLC system, coupled to an Orbitrap Velos Pro (Thermo Scientific) mass spectrometer with electrospray ion source. Peptides were separated by gradient elution using water as mobile phase A, and acetonitrile as mobile phase B, both containing 0.1% formic acid. The gradient elution used was as follows: 0−2 min 3% B; 2−85 min 3−50% B; 83−83.1 min 50−95% B; 83.1−85 min 95% B; 85−85.1 min 95−3% B and 85.1−90 min 3% B. The Orbitrap Velos was operated in information dependent acquisition (IDA) mode with CID performed on the top 10 ions. The MS scan was performed in the Orbitrap at 100 000 resolution, whereas the fragment spectra were collected in the low pressure trap. Ion trap and Orbitrap maximal injection times were set to 50 and 500 ms, respectively. The ion target values were 30 000 for the ion trap, and 1 000 000 for the Orbitrap.

In Vitro Stability and Protease Inhibitor Assays. Plasma samples from mouse, rat, cynomolgus monkey, and human were purchased from BioreclamationIVT. In vitro stability assays were carried out by incubating 0.125 mg/mL of ADC in 62.5% (v/v) plasma diluted in 1× PBS. Protease inhibitors (Roche, Sigma) were added to plasma at appropriate concentrations as needed. In some assays, pH was adjusted by addition of 120 mM sodium acetate pH 5.2, 120 mM potassium phosphate pH 6.0 or 7.4, or 120 mM Tris HCl pH 8.5. Following incubation at 37 °C for 20 h − 4.5 days, samples were diluted with an equal volume of 1× PBS, and conjugates were isolated using MabSelect SuRe beads or M1S1 antigen coupled to CNBr-activated Sepharose

DOI: 10.1021/bc5005747
Bioconjugate Chem. 2015, 26, 650−659

(GE Healthcare, Inc.) following standard protocols. DAR values were assessed using HIC or mass spectrometric methods.

In Vivo Stability Assays. Plasma samples were obtained from mice 4.5 days following injection with 3 mg/kg cleavable ADCs. Samples were diluted with an equal volume of 1× PBS pH 7.4, and conjugates were isolated using MabSelect SuRe beads or M1S1 antigen coupled to CNBr-activated Sepharose (GE Healthcare, Inc.) following standard protocols. DAR values were assessed using HIC or mass spectrometric methods.

Enzymatic Assays. Purified recombinant mouse and human Cathepsin B were purchased from R&D Systems. Purified human Cathepsin B from liver was purchased from Sigma. Enzymes were activated in the presence of 1.2 mM L-cysteine and 0.75 mM EDTA at 40 °C for 10 min, and 0.5 ug/mL of enzyme was reacted with 0.125 mg/mL C16 Site A-C6-VC-PABC-Aur0101 substrate in one of the following buffers: 120 mM sodium acetate pH 5.2, 120 mM potassium phosphate pH 6.0 or 7.4, or 120 mM Tris HCl pH 8.5. Appropriate concentrations of protease inhibitors (Roche, Sigma) and 52.5% (v/v) mouse or human plasma (Bioreclamation) were added to reactions prior to the addition of substrate as desired. Following incubation at 37 °C for 20 h, conjugate was isolated using MabSelect SuRe beads or M1S1 antigen coupled to CNBr-activated Sepharose (GE Healthcare, Inc.) following standard protocols. DAR values were assessed using HIC or mass spectrometric methods.

In Vitro Cytotoxicity Assays. In vitro cytotoxicity studies of anti-M1S1 ADCs were performed on the high target-expressing pancreatic adenocarcinoma BxPC3 cell line (M1S1+++), and the target-negative colorectal adenocarcinoma SW620 cell line (M1S1-). Cells were seeded on white-walled clear-bottom plates at 2000 cells per well 24 h before treatment. Cells were treated with 4-fold serially diluted ADCs in triplicate. Cell viability was determined by CellTiter-Glo Luminescent Cell Viability Assay 96 (Promega, Madison, WI) 96 h after treatment. Relative cell viability was determined as percentage of untreated control. IC_{50} values were calculated by GraphPad Prism 5 software.

In Vivo Efficacy Studies. In vivo efficacy studies of ADCs with different stabilities were performed with the high target-expressing BxPC3 (M1S1+++) xenograft model. Two million BxPC3 cancer cells were implanted subcutaneously into 5−8 weeks old female CB17 SCID mice, and tumor growth was monitored until the tumor sizes reached around 200 mm^3. Animals were randomized by tumor sizes into groups of 4−5, and a single dose of either 3 mg/kg or 1.5 mg/kg of cleavable ADC was administered through bolus tail vein injection. Tumor volume was measured twice a week by a Caliper device and calculated with the following formula: Tumor volume = (length × $width^2$)/2. Animals were euthanized once tumor volumes reached 2000 mm^3.

Pharmacokinetics and in Vivo Stability Studies. For PK and stability experiments, compounds were dosed IV through the lateral tail vein at 3 mg/kg, and samples were withdrawn via retro-orbital bleed under isoflurane anesthesia at appropriate time points. For pharmacokinetic studies, a single intravenous dose of 3 mg/kg of ADC was administered into female CB17 SCID mice (n = 3). Stability samples were obtained from the same group at terminal bleeds.

Total Antibody PK Assay. Each well of a 96-well microtiter plate (NUNC) was coated with 100 uL of goat anti-human IgG antibody Fc specific (Pierce cat# 31125) at 1 ug/mL in 1× PBS (Cell Gro). The plates were incubated at 4−8 °C overnight. All washing steps were performed with a Biotek ELx405 plate washer with 1× PBS/0.05% Tween. After washing 3 times, plates were blocked with 200 uL of assay buffer (1× PBS/0.5% BSA/0.05% Polysorbate 20) and incubated for 1−2 h at room temperature with gentle agitation. Plates were washed 3 times and 100 μL of standards, controls, and samples diluted 1:100 in assay buffer were added to the corresponding wells. After a 2 h incubation with gentle agitation at room temperature, plates were washed 6 times before dispensing 100 μL of the detection antibody (anti-human IgG, Fab specific, HRP-labeled from Sigma, cat#A0293) diluted to 250 ng/mL in assay buffer. The plates were incubated for one more hour with gentle agitation at room temperature before washing 6 times. Then, 100 μL of TMB (KPL, SureBlue) was added to each well. Color development was allowed for approximately 5 min before stopping the reaction with 100 μL of 1 M phosphoric acid. Absorbance was measured at 450 nm with a reference at 650 nm on a SpectraMax 340 plate reader (Molecular Devices). SoftMax Pro 5.2 software was used to fit standard curves with a 4-parameter regression, and to calculate sample concentrations.

ADC PK Assay. Each well of a 96-well microtiter plate (NUNC) was coated with 100 μL of goat anti-human IgG antibody at 2 μg/mL in 1× PBS (Cell Gro). The plates were incubated at 4−8 °C overnight. All washing steps were performed on a Biotek ELx405 plate washer with 1× PBS/0.05% Tween. After washing 3 times, plates were blocked with 200 μL/well of assay buffer (1× PBS/0.5% BSA/0.05% Polysorbate 20) and incubated for 1−2 h at room temperature with gentle agitation. Plates were washed 3 times and 100 μL of standards, controls, and samples diluted 1:100 in assay buffer were added in duplicate to the corresponding wells. After a 2 h incubation with gentle agitation at room temperature, plates were washed 6 times before dispensing 100 μL of the detection antibody (biotinylated anti-MMAD monoclonal antibody, Pfizer) diluted to 4 μg/mL in assay buffer. The plates were incubated for 1.5 h with gentle agitation at room temperature before washing 6 times. Avidin-HRP (Vector, cat A-2004) was diluted to 0.25 μg/mL in assay buffer and 100 μL was dispensed into each well. Plates were incubated for another hour before washing 6 times. Then, 100 μL of TMB (KPL, SureBlue) was added to each well. Color development was allowed for approximately 5 min before stopping the reaction with 100 μL of 1 M phosphoric acid. Absorbance was measured at 450 nm with a reference at 650 nm on a SpectraMax 340 plate reader (Molecular Devices). SoftMax Pro 5.2 software was used to fit standard curves with a 4-parameter regression, and to calculate sample concentrations.

Chemical Synthesis. Synthesis of C6-VC-PABC-MMAD (AmCapValCitPABC-MMAD) was previously described.[7] Synthesis of C6-VC-PABC-Aur0101 (AmCapValCitPABC-Auristatin-0101) was as follows:

*Fmoc-AmCapValCitPABA-OH (**2**).* A solution of Fmoc-6-aminohexanoic acid (4.2 g, 11.40 mmol) in anhydrous *N,N*-dimethylformamide (50 mL) was treated with *N,N*-diisopropylethylamine (3.8 mL, 2.82 g, 21.8 mmol, 1.8 equiv) and HATU (5.6 g, 14.75 mmol, 1.25 equiv) and the mixture was stirred at room temperature for 10 min. L-Valyl-N^5-carbamoyl-*N*-[4-(hydroxymethyl)phenyl]-L-ornithinamide[11] (5.6 g, 14.75 mmol, 1.25 equiv) was then added to the mixture and stirring was continued for 15 h at room temperature. Dichloromethane was added to precipitate the product, which was filtered and air-dried to provide 5.9 g (100%) of the desired material as an off-white solid. This material was used directly in subsequent reactions without further purification. MS (ES) m/z: 715.6 $[M + H]^+$.

*Fmoc-AmCapValCitPABC-PNP (**3**).* A solution of FmocAmCapValCitPABA-OH (500 mg, 0.7 mmol) and bis(4-nitrophenyl)carbonate (638 mg, 2.1 mmol, 3 equiv) in anhydrous

DOI: 10.1021/bc5005747
Bioconjugate Chem. 2015, 26, 650−659

N,N-dimethylformamide (3 mL) was treated with *N,N*-diisopropylethylamine (365 μL, 270 mg, 2.1 mmol, 3 equiv) and the reaction was stirred at room temperature overnight. The reaction mixture was concentrated in vacuo and the resulting residue was purified by silica gel chromatography using gradient elution of 0−25% methanol in dichloromethane over 15 min, followed by isocratic elution of 25% methanol in dichloromethane. Pooled product-containing fractions were evaporated to provide 402 mg (68%) of the desired product as an off-white solid. MS (ES) m/z: 880.3 $[M + H]^+$.

*N-(6-Aminohexanoyl)-L-valyl-N-{4-[(8S,11S,12R)-11-[(2S)-butan-2-yl]-12-(2-{(2S)-2-[(1R,2R)-1-methoxy-2-methyl-3-oxo-3-{[(1S)-2-phenyl-1-(1,3-thiazol-2-yl)ethyl] amino}propyl]pyrrolidin-1-yl}-2-oxoethyl)-5,5,10-trimethyl-3,6,9-trioxo-8-(propan-2-yl)-2,13-dioxa-4,7,10-triazatetradec-1-yl]phenyl}-N^5-carbamoyl-L-ornithinamide (AmCapValCitPABC-Auristatin-0101, **5**).* A solution of 2-methylalanyl-*N*-[(3*R*,4*S*,5*S*)-3-methoxy-1-{(2*S*)-2-[(1*R*,2*R*)-1-methoxy-2-methyl-3-oxo-3-{[(1*S*)-2-phenyl-1-(1,3-thiazol-2-yl)ethyl]amino}propyl]pyrrolidin-1-yl}-5-methyl-1-oxoheptan-4-yl]-*N*-methyl-L-valinamide[10] (105 mg, 0.141 mmol), FmocAmCapValCitPABC-PNP (138 mg, 0.157 mmol), HOAt (6.40 mg, 0.047 mmol), and 2,6-lutidine (91 uL, 84 mg, 0.783 mmol) in *N,N*-dimethylformamide (1.4 mL) was heated at 45 °C for 21 h. Additional FmocAmCapValCitPABC-PNP (31 mg, 0.035 mmol), HOAt (3.83 mg, 0.028 mmol), and 2,6-lutidine (16 uL, 15 mg, 0.141 mmol) were then added, the reaction was heated at 40 °C for an additional 6 h, and then kept at room temperature overnight. LCMS analysis indicated that the reaction contained a mixture of compounds **4** and **5**. Piperidine (0.5 mL) was added and the reaction stirred at room temperature for 1 h. LCMS analysis indicated that the Fmoc-deprotection reaction was complete, and the reaction was concentrated and the residue was and purified by reverse phase chromatography over a 100 × 30 mm^2, 5 μm Phenomenex Luna C18 column using flow rate of 20 mL/min and gradient elution of 10−85% acetonitrile in water containing 0.02% trifluoracetic acid over 20 min. Pooled product-containing fractions were concentrated and lyophilized to provide 97 mg (54%) of the desired product (**5**) as white solid. MS (ES): m/z 1062.3$[M + H]^+$. This material was greater than 95% pure by analytical HPLC and the ^{1}H NMR was consistent with the assigned structure.

■ ASSOCIATED CONTENT

Ⓢ Supporting Information

Cytotoxicity of untreated and plasma-treated cleavable conjugates against the BxPC3 cell line (M1S1+++). Inhibition of Cathepsin B-catalyzed cleavage of the C16 Site A-C6-VC-PABC-Aur0101 substrate upon addition of mouse or human plasma. Stability analysis of the cleavable C16 Site A-C6-VC-PABC-Aur0101 conjugate using hydrophobic interaction chromatography. Mass spectrometric analysis of the cleavage product of C16 Site A-C6-VC-PABC-Aur0101 conjugate isolated from mouse plasma. Cytotoxicity assays of cleavable C6-VC-PABC-Aur0101 conjugates across various sites. Correlation between changes in IC_{50} values (efficacy) and changes in DAR (stability) for cleavable conjugates incubated in mouse plasma. Pharmacokinetic profiles of the humanized C16 Site D-C6-VC-PABC-MMAD conjugate in rat, and the chimeric C16 Site D-C6-VC-PABC-MMAD conjugate in cynomolgus monkey. This material is available free of charge via the Internet at http://pubs.acs.org.

■ AUTHOR INFORMATION

Corresponding Author

*E-mail: pavel.strop@pfizer.com. Phone: (650) 615-7355.

Author Contributions

Magdalena Dorywalska and Pavel Strop contributed equally to the work.

Notes

The authors declare the following competing financial interest(s): All authors are employees of Pfizer Inc.

■ ACKNOWLEDGMENTS

We would like to thank Michael Sherman Chin, Teresa Wong, and Colleen Brown for cell culture support, and Dan McDonough for help with ELISA assays. We also thank Janette Sutton for assistance with PK and stability experiments, and Eugenia Kraynov for help with PK studies.

■ REFERENCES

(1) Lambert, J. M. (2013) Drug-conjugated antibodies for the treatment of cancer. *Br. J. Clin. Pharmacol. 76*, 248−62.

(2) Sievers, E. L., and Senter, P. D. (2013) Antibody-drug conjugates in cancer therapy. *Annu. Rev. Med. 64*, 15−29.

(3) Panowksi, S., Bhakta, S., Raab, H., Polakis, P., and Junutula, J. R. (2014) Site-specific antibody drug conjugates for cancer therapy. *MAbs 6*, 34−45.

(4) Doronina, S. O., Toki, B. E., Torgov, M. Y., Mendelsohn, B. A., Cerveny, C. G., Chace, D. F., DeBlanc, R. L., Gearing, R. P., Bovee, T. D., Siegall, C. B., Francisco, J. A., Wahl, A. F., Meyer, D. L., and Senter, P. D. (2003) Development of potent monoclonal antibody auristatin conjugates for cancer therapy. *Nat. Biotechnol. 21*, 778−84.

(5) Sanderson, R. J., Hering, M. A., James, S. F., Sun, M. M., Doronina, S. O., Siadak, A. W., Senter, P. D., and Wahl, A. F. (2005) In vivo drug-linker stability of an anti-CD30 dipeptide-linked auristatin immunoconjugate. *Clin. Cancer. Res. 11*, 843−52.

(6) Strop, P., Dorywalska, M., Rajpal, A., Shelton, D. L., Liu, S.-H., Pons, J., and Dushin, R. (2012) Patent WO2012059882.

(7) Strop, P., Liu, S. H., Dorywalska, M., Delaria, K., Dushin, R. G., Tran, T. T., Ho, W. H., Farias, S., Casas, M. G., Abdiche, Y., Zhou, D., Chandrasekaran, R., Samain, C., Loo, C., Rossi, A., Rickert, M., Krimm, S., Wong, T., Chin, S. M., Yu, J., Dilley, J., Chaparro-Riggers, J., Filzen, G. F., O'Donnell, C. J., Wang, F., Myers, J. S., Pons, J., Shelton, D. L., and Rajpal, A. (2013) Location matters: site of conjugation modulates stability and pharmacokinetics of antibody drug conjugates. *Chem. Biol. 20*, 161−7.

(8) Farias, S. E., Strop, P., Delaria, K., Galindo Casas, M., Dorywalska, M., Shelton, D. L., Pons, J., and Rajpal, A. (2014) Mass spectrometric characterization of transglutaminase based site-specific antibody-drug conjugates. *Bioconjugate Chem. 25*, 240−50.

(9) Shen, B. Q., Xu, K., Liu, L., Raab, H., Bhakta, S., Kenrick, M., Parsons-Reponte, K. L., Tien, J., Yu, S. F., Mai, E., Li, D., Tibbitts, J., Baudys, J., Saad, O. M., Scales, S. J., McDonald, P. J., Hass, P. E., Eigenbrot, C., Nguyen, T., Solis, W. A., Fuji, R. N., Flagella, K. M., Patel, D., Spencer, S. D., Khawli, L. A., Ebens, A., Wong, W. L., Vandlen, R., Kaur, S., Sliwkowski, M. X., Scheller, R. H., Polakis, P., and Junutula, J. R. (2012) Conjugation site modulates the in vivo stability and therapeutic activity of antibody-drug conjugates. *Nat. Biotechnol. 30*, 184−9.

(10) Maderna, A., Doroski, M., Subramanyam, C., Porte, A., Leverett, C. A., Vetelino, B. C., Chen, Z., Risley, H., Parris, K., Pandit, J., Varghese, A. H., Shanker, S., Song, C., Sukuru, S. C., Farley, K. A., Wagenaar, M. M., Shapiro, M. J., Musto, S., Lam, M. H., Loganzo, F., and O'Donnell, C. J. (2014) Discovery of cytotoxic dolastatin 10 analogues with N-terminal modifications. *J. Med. Chem. 57*, 10527−43.

(11) Dubowchik, G. M., Firestone, R. A., Padilla, L., Willner, D., Hofstead, S. J., Mosure, K., Knipe, J. O., Lasch, S. J., and Trail, P. A. (2002) Cathepsin B-labile dipeptide linkers for lysosomal release of doxorubicin from internalizing immunoconjugates: model studies of enzymatic drug release and antigen-specific in vitro anticancer activity. *Bioconjugate Chem. 13*, 855−69.

(12) Toki, B. E., Cerveny, C. G., Wahl, A. F., and Senter, P. D. (2002) Protease-mediated fragmentation of p-amidobenzyl ethers: a new

DOI: 10.1021/bc5005747
Bioconjugate Chem. 2015, 26, 650−659

strategy for the activation of anticancer prodrugs. *J. Org. Chem. 67*, 1866−72.
(13) Doronina, S. O., Bovee, T. D., Meyer, D. W., Miyamoto, J. B., Anderson, M. E., Morris-Tilden, C. A., and Senter, P. D. (2008) Novel peptide linkers for highly potent antibody-auristatin conjugate. *Bioconjugate Chem. 19*, 1960−3.
(14) Sutherland, M. S., Sanderson, R. J., Gordon, K. A., Andreyka, J., Cerveny, C. G., Yu, C., Lewis, T. S., Meyer, D. L., Zabinski, R. F., Doronina, S. O., Senter, P. D., Law, C. L., and Wahl, A. F. (2006) Lysosomal trafficking and cysteine protease metabolism confer target-specific cytotoxicity by peptide-linked anti-CD30-auristatin conjugates. *J. Biol. Chem. 281*, 10540−7.
(15) Weidle, U. H., Tiefenthaler, G., and Georges, G. (2014) Proteases as activators for cytotoxic prodrugs in antitumor therapy. *Cancer Genomics Proteomics 11*, 67−79.
(16) Hook, V. Y. (2006) Unique neuronal functions of cathepsin L and cathepsin B in secretory vesicles: biosynthesis of peptides in neurotransmission and neurodegenerative disease. *Biol. Chem. 387*, 1429−39.
(17) Sundelof, J., Sundstrom, J., Hansson, O., Eriksdotter-Jonhagen, M., Giedraitis, V., Larsson, A., Degerman-Gunnarsson, M., Ingelsson, M., Minthon, L., Blennow, K., Kilander, L., Basun, H., and Lannfelt, L. (2010) Higher cathepsin B levels in plasma in Alzheimer's disease compared to healthy controls. *J. Alzheimers Dis. 22*, 1223−30.
(18) Vasiljeva, O., Reinheckel, T., Peters, C., Turk, D., Turk, V., and Turk, B. (2007) Emerging roles of cysteine cathepsins in disease and their potential as drug targets. *Curr. Pharm. Des. 13*, 387−403.
(19) Fonovic, M., and Turk, B. (2014) Cysteine cathepsins and extracellular matrix degradation. *Biochim. Biophys. Acta 1840*, 2560−70.
(20) Reiser, J., Adair, B., and Reinheckel, T. (2010) Specialized roles for cysteine cathepsins in health and disease. *J. Clin. Invest. 120*, 3421−31.
(21) Yan, S., and Sloane, B. F. (2003) Molecular regulation of human cathepsin B: implication in pathologies. *Biol. Chem. 384*, 845−54.
(22) Mohamed, M. M., and Sloane, B. F. (2006) Cysteine cathepsins: multifunctional enzymes in cancer. *Nat. Rev. Cancer 6*, 764−75.
(23) Guha, S., and Padh, H. (2008) Cathepsins: fundamental effectors of endolysosomal proteolysis. *Indian J. Biochem. Biophys. 45*, 75−90.
(24) Roche Molecular Biochemicals, *The Complete Guide for Protease Inhibition*.
(25) Sigma-Aldrich. (2009) Protease Inhibition and Detection. *Life Science BioFiles 4*.
(26) Smyth, D. G., Blumenfeld, O. O., and Konigsberg, W. (1964) Reactions of N-ethylmaleimide with peptides and amino acids. *Biochem. J. 91*, 589−95.
(27) Snellman, O., and Sylven, B. (1967) Haptoglobin acting as a natural inhibitor of cathepsin B activity. *Nature 216*, 1033.
(28) Ducry, L., and Stump, B. (2010) Antibody-drug conjugates: linking cytotoxic payloads to monoclonal antibodies. *Bioconjugate Chem. 21*, 5−13.
(29) Cardillo, T. M., Govindan, S. V., Sharkey, R. M., Trisal, P., and Goldenberg, D. M. (2011) Humanized anti-Trop-2 IgG-SN-38 conjugate for effective treatment of diverse epithelial cancers: preclinical studies in human cancer xenograft models and monkeys. *Clin. Cancer Res. 17*, 3157−69.
(30) Alley, S. C., Benjamin, D. R., Jeffrey, S. C., Okeley, N. M., Meyer, D. L., Sanderson, R. J., and Senter, P. D. (2008) Contribution of linker stability to the activities of anticancer immunoconjugates. *Bioconjugate Chem. 19*, 759−65.
(31) Tumey, L. N., Charati, M., He, T., Sousa, E., Ma, D., Han, X., Clark, T., Casavant, J., Loganzo, F., Barletta, F., Lucas, J., and Graziani, E. I. (2014) Mild method for succinimide hydrolysis on ADCs: impact on ADC potency, stability, exposure, and efficacy. *Bioconjugate Chem. 25*, 1871−80.
(32) Lyon, R. P., Setter, J. R., Bovee, T. D., Doronina, S. O., Hunter, J. H., Anderson, M. E., Balasubramanian, C. L., Duniho, S. M., Leiske, C. I., Li, F., and Senter, P. D. (2014) Self-hydrolyzing maleimides improve the stability and pharmacological properties of antibody-drug conjugates. *Nat. Biotechnol. 32*, 1059−62.
(33) Tian, F., Lu, Y., Manibusan, A., Sellers, A., Tran, H., Sun, Y., Phuong, T., Barnett, R., Hehli, B., Song, F., DeGuzman, M. J., Ensari, S., Pinkstaff, J. K., Sullivan, L. M., Biroc, S. L., Cho, H., Schultz, P. G., DiJoseph, J., Dougher, M., Ma, D., Dushin, R., Leal, M., Tchistiakova, L., Feyfant, E., Gerber, H. P., and Sapra, P. (2014) A general approach to site-specific antibody drug conjugates. *Proc. Natl. Acad. Sci. U. S. A. 111*, 1766−71.
(34) Jeger, S., Zimmermann, K., Blanc, A., Grünberg, J., Honer, M., Hunziker, P., Struthers, H., and Schibli, R. (2010) Site-specific and stoichiometric modification of antibodies by bacterial transglutaminase. *Angew. Chem. Int. Ed. Engl. 49*, 9995−9997.

DOI: 10.1021/bc5005747
Bioconjugate Chem. 2015, 26, 650−659